Journal Pre-proof

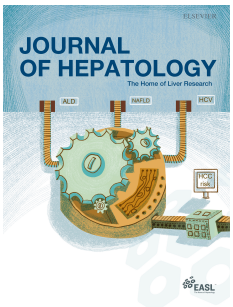

A single-cell atlas of the woodchuck liver reveals cellular programs conserved in human HBV infection

Zoe A. Clarke, Jawairia Atif, Xinle Wang, Lewis Y. Liu, Lawrence Wood, Damra Camat, Yijia Liu, Ariya Shiwram, Sharon J. Hyduk, Sai Chung, Xue-Zhong Ma, Justin Manuel, Si Lok, Timothy N.H. Lau, Cornelia Thoeni, Tomasz I. Michalak, Ian D. McGilvray, Gary D. Bader, Sonya A. MacParland

PII: S0168-8278(26)00019-X

DOI: https://doi.org/10.1016/j.jhep.2025.12.030

Reference: JHEPAT 10401

To appear in: *Journal of Hepatology*

Received Date: 9 January 2025

Revised Date: 27 December 2025

Accepted Date: 29 December 2025

Please cite this article as: Clarke ZA, Atif J, Wang X, Liu LY, Wood L, Camat D, Liu Y, Shiwram A, Hyduk SJ, Chung S, Ma XZ, Manuel J, Lok S, Lau TNH, Thoeni C, Michalak TI, McGilvray ID, Bader GD, MacParland SA, A single-cell atlas of the woodchuck liver reveals cellular programs conserved in human HBV infection, *Journal of Hepatology*, https://doi.org/10.1016/j.jhep.2025.12.030.

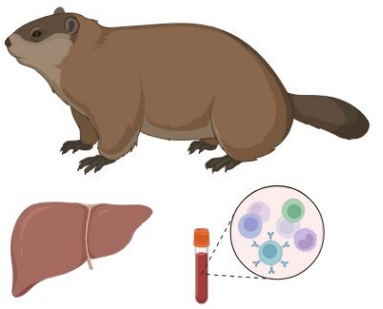

Healthy woodchuck liver and PBMCs

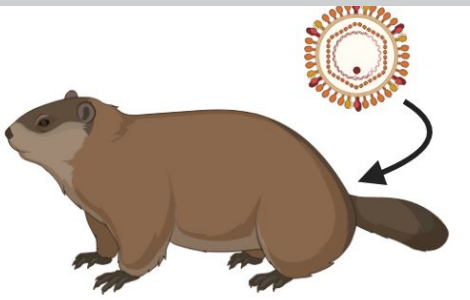

Chronic woodchuck hepatitis virus (cWHV) liver and PBMCs

Precision cut liver slices (PCLS): PMA/ionomycin stimulation

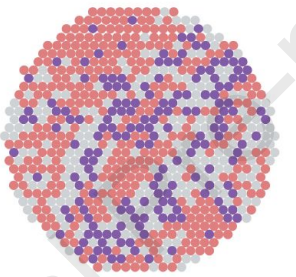

Spatial transcriptomics

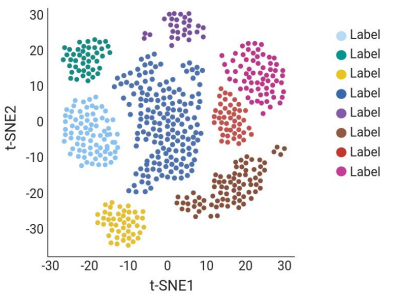

Single-cell transcriptomics

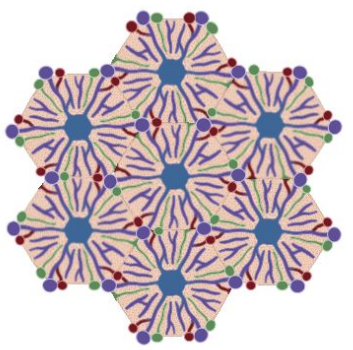

Characterizing cellular diversity and transcriptomics signatures of woodchuck PBMC and liver cells

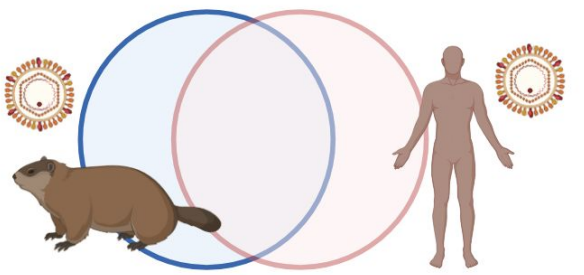

Overlapping pathways between cWHV infected tissue and HBV infected tissue

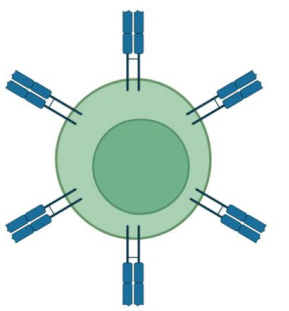

Enrichment of disease-related intrahepatic *PDCD1+, IFNG+, TIGIT+, TOX+, CD8A+* T cells in cWHV/HBV infection

A single-cell atlas of the woodchuck liver reveals cellular programs conserved in human HBV infection

Short title: Woodchuck liver map shows conserved human biology

Zoe A. Clarke[1,2#], Jawairia Atif[3,4#], Xinle Wang[3#], Lewis Y. Liu[3,4], Lawrence Wood[3,4], Damra Camat[3,4], Yijia Liu[6], Ariya Shiwram[3], Sharon J. Hyduk[4], Sai Chung[3,4], Xue-Zhong Ma[4], Justin Manuel[4], Si Lok[5], Timothy N. H. Lau[5], Cornelia Thoeni[6], Tomasz I. Michalak[7], Ian D. McGilvray[4*], Gary D. Bader[1,2,8*], Sonya A. MacParland[3,4,6*]

Affiliations:

1 - Department of Molecular Genetics, University of Toronto, Toronto, Ontario, Canada

2 - The Donnelly Centre, University of Toronto, Toronto, Ontario, Canada

3 - Department of Immunology, University of Toronto, Toronto, Ontario Canada

4 - Ajmera Transplant Centre, Toronto General Hospital Research Institute, Toronto, Ontario, Canada

5 - The Centre for Applied Genomics, The Hospital for Sick Children, Toronto, Ontario, Canada

6 - Department of Laboratory Medicine and Pathobiology, University of Toronto, Toronto, Ontario, Canada

7 - Molecular Virology and Hepatology Research Group, Faculty of Medicine, Health Science Center, Memorial University of Newfoundland, St. John's, Newfoundland, Canada

8 - Department of Computer Science, University of Toronto, Toronto, Ontario, Canada

#equal contribution co-first authors.

*Equal contribution senior authors

Corresponding author: Sonya MacParland (s.macparland@utoronto.ca)

Keywords: Liver, Single Cell RNA sequencing, Spatial Transcriptomics, Single Nucleus RNA sequencing, Woodchuck, Marmota monax

Electronic Word Count: 5,975 words

Number of Figures and Tables: 7

Conflicts of Interest: None to declare

Financial Support Statement: We acknowledge the University of Toronto McLaughlin Centre Accelerator Grants in Genomic Medicine awarded to I.D.M., G.D.B., S.A.M. the Canadian Liver Foundation's Team Grant in Hepatocellular Carcinoma to I.D.M., T.I.M., W.C.W.C., S.A.M., the UHN Foundation, and the Natural Sciences and Engineering Research Council (NSERC) Discovery Grant program RGPIN-2018-05958 to S.A.M. and the Canadian Institutes for Health Research (grant PJT 469829) to G.D.B.. J.A. has received a graduate student fellowship from the Canadian Network on Hepatitis C (CanHepC). CanHepC is funded by a joint initiative of the Canadian Institutes of Health Research (CIHR) (NHC-142832) and the Public Health Agency of Canada (PHAC). The Woodchuck reference genome was generated based on sequencing funded through the

CanSeq150 program of CGEn, Canada's national platform for genome sequencing and analysis.

Author Contributions: S.A.M., G.D.B., and I.D.M. designed the study. S.L. and T.L. sequenced the genome. Z.A.C. annotated the genome. L.Y.L., D.C., S.C., X.-Z.M., L.W. and J.M. conducted liver experiments. Z.A.C. and J.A. performed the computational analysis. Z.A.C., X.W., T.I.M., and J.A. interpreted the data. C. T. performed the pathological review on the IHC. All authors contributed to the writing of the paper.

Data Availability:

The woodchuck genome sequence and annotation are available at https://doi.org/10.5281/zenodo.10855128. The raw RNA-seq data and data matrices output by Cell Ranger are available at the Gene Expression Omnibus (GEO) at accession numbers GSE264104 (scRNA-seq), GSE264107 (spatial), and GSE264112 (snRNA-seq). The single-cell and single-nucleus datasets are hosted by UCSC Cell Pre-publication browser (https://cells-test.gi.ucsc.edu/?ds=woodchuck-liver), final post publication browser at https://woodchuck-liver.cells.ucsc.edu. The code used to process the data can be found at https://github.com/14zac2/HealthyWoodchuckMap

Abstract:

Background: The eastern woodchuck (Marmota monax), which can be naturally infected with woodchuck hepatitis virus (WHV), has served as a model for aspects of human hepatitis B virus (HBV) infection, including the establishment of chronic infection and progression from chronic hepatitis to liver cancer. However, the cellular landscape of the woodchuck liver and its parallels to HBV infection remain uncharacterized.

Methods: We present a woodchuck single-cell and spatial transcriptomic atlas in health and chronic WHV infection, with a characterization of cell-type and infection-driven processes in hepatic (Healthy: 52,024 cells; Infected: 40,810 cells; n=8 each) and peripheral blood mononuclear cells (Healthy: 25,314 cells, n=7; Infected: 19,518 cells, n=8). We further examined shared WHV–HBV disease pathways transcriptionally and assessed woodchuck liver immune responses functionally using precision-cut woodchuck liver slice stimulation.

Results: We applied our generated atlas and found hepatic cellular and immune diversity in woodchuck liver was comparable to human livers. We found that immune cells in the PMA/IONO stimulated PCLS displayed a type I inflammatory response as expected, reinforcing our annotations. Our atlas further demonstrated transcriptional and cellular similarities between the HBV and WHV infected liver, including the activation of dendritic cells in the periportal region of the infected liver, and a restructuring of the T cell compartment in WHV infection from memory towards exhaustion, a hallmark of human HBV.

Conclusions: We present a multi-omic atlas of healthy, diseased, and ex vivo–stimulated woodchuck liver. This work identified shared WHV–HBV pathological processes, reinforces the value of this preclinical model and provides a resource to advance HBV pathogenesis studies and therapeutic development.

Impact and Implications:

Limited treatment options for liver disease, often requiring liver transplantation, emphasize the need for human-relevant animal models to speed the development of new therapeutic interventions. Woodchucks infected with woodchuck hepatitis virus (WHV) develop chronic hepatitis and liver cancer, similar to human hepatitis B virus (HBV) infection. However, the composition and active biological processes in woodchuck hepatic cells were poorly understood, limiting the utility of this model to therapeutic discovery. In this study, we characterized the healthy and chronically infected woodchuck liver in comparison to human HBV at a single-cell resolution reinforcing the potential of WHV-infected woodchuck as a model for human HBV disease.

Introduction

The mammalian liver is a vital organ with essential metabolic and detoxification functions.[1–3] It has a profound regenerative capacity that can be compromised in end-stage disease, necessitating transplantation.[4] The hepatitis B virus (HBV) is a

hepatotrophic virus that can persist chronically in the infected host and can lead to hepatocellular carcinoma (HCC), the most common primary form of liver cancer.[5]

Investigations into the pathogenesis of HBV have been constrained by limited access to physiologically relevant animal models, restricted human tissue availability, and the inherent fragility of hepatic cell populations.[1,6] While single-cell RNA sequencing (scRNA-seq) and spatial transcriptomics have advanced our understanding of hepatic cellular complexity, the lack of a well-characterized HBV animal model precludes functional studies of disease progression and therapeutic intervention.[1,7]

The eastern North American woodchuck, *Marmota monax*, can be naturally infected with woodchuck hepatitis virus (WHV) and serves as a critical immunocompetent preclinical model for HBV-induced liver disease.[8,9] WHV mirrors human HBV in genome organization, and the infection causes an immune response, and disease progression from hepatitis to HCC reflective of human disease.[8,9] This model has helped reveal key insights in chronic HBV persistence, but its full potential is limited by scarce woodchuck-specific cell biology resources for tracking cellular ecosystems during WHV infection.[10–12]

Here, we mapped the healthy and WHV-infected woodchuck liver and matched peripheral blood mononuclear cells (PBMCs) using scRNA-seq, spatial transcriptomics, and *in-vitro* tissue stimulation studies (Fig. 1). We applied this map to examine WHV-induced disease pathways and identified overlapping T cell exhaustion and dendritic cell differentiation and activation pathways in chronic WHV (cWHV)-infected woodchuck livers and human chronic HBV (cHBV) infection, including *TIGIT*, *TOX*, *PDCD1*, and *IFNG*. This analysis provides a foundation for cell-specific studies of HBV liver

pathogenesis and oncogenesis, and for preclinical evaluation of new therapies for cHBV and HCC.

Methods

Detailed methods of tissue and transcriptomic data processing and data analysis can be found in the supplementary methods.

Tissue preparation

All animal procedures included in this study were approved by institutional ethics boards (supplementary methods). Woodchucks (see clinical and virological characteristics, Table S1) were infected with WHV under established protocols and liver tissue was dissociated into single-cell suspensions as previously described.[1,13] PBMCs were isolated using standard percoll-based density gradient centrifugation.

Precision-cut woodchuck liver slice stimulations

Precision-cut liver slices were generated from woodchuck W3391 (healthy) and stimulated for *ex vivo* studies as previously described and single-nucleus RNA-seq (snRNA-seq) of stimulated slices was performed.

RNA-sequencing and data processing

We developed a new, annotated high-quality woodchuck genome annotation to enable gene identification and quantification from RNA-sequencing data (Fig. S1, details in supplementary methods). 3' Visium spatial transcriptomics (10x Genomics, see Table S2- for sample QC) was performed on OCT-embedded 16-micron slices each

from a healthy (L212) and diseased (L215) woodchuck liver tissue) and scRNA-seq and snRNA-seq data (10X Genomics chromium SingleCell 3' v2 chemistry) were aligned to the woodchuck genome using 10X Genomics Space Ranger v1.2.2 and 10X Genomics Cell Ranger v5.0.0[14] respectively. Sequencing data were processed, integrated, and annotated using the seurat v5 analysis[14] pipeline, and DropletQC[15] was used to remove empty droplets in filtered Cell Ranger results (Fig. S2 and Fig. S3). Shared immune dysfunction between cWHV and cHBV infections was examined *via* pathway analysis using publicly available human HBV data (GSE182159)[16].

DNA extraction and quantitative WHV PCR

DNA was isolated from 100 µL plasma or 10 mg of snap-frozen tissue and was amplified by quantitative polymerase chain reaction (qPCR) using WHV and woodchuck b-actin specific primers. Cycling conditions were as follows: 95 °C for 1 min followed by 45 amplification cycles (95 °C for 15 s, 60 °C for 30 s) and a melt curve. Primers against the WHV preS region were used at a final concentration of 250nM (forward: ATGCACCCATTCTCTCGAC; reverse: CTGAGCAGCTTGGTTAGAGT). Standard curves were generated using serial dilutions of WHV plasmid DNA from 108 to 1 copies/reaction. The WHV viral copies are reported as copies per mL of plasma or ng of total DNA. Full details can be found in supplementary methods.

Results

An Atlas of Healthy Woodchuck Liver Cells and PBMCs Demonstrates Compartment Specific Immune Subtypes and Transcriptional Profiles

After filtering, scRNA-seq of six liver biopsies and two perfused lobes yielded 52,024 liver cells and 25,314 PBMCs, which were broadly grouped into 24 cell types (Fig. 2A-E, Fig. S4). Our combined atlas of woodchuck liver and PBMC was annotated with automated methods based on human datasets,[1,2,17,18] (Fig. S5) and manual curation focused on lineage-associated genes from human liver single-cell studies (Table S3, Fig. S6-S10). Our approach to include biopsies and perfused caudates captured both liver parenchymal (hepatocytes and cholangiocytes) and non-parenchymal cell populations (endothelial and mesenchymal cells, Fig. S6-7), and immune cell populations (myeloid cells, T cells, NK cells, and mature and antibody-secreting B cells, Fig. S8-10) based on transcriptomic similarity to their human counterparts (Fig. S5).

With these annotations applied (Fig. 2A), we first employed the atlas to examine infiltrating immune cells in woodchuck liver homogenates *vs* those found in PBMCs to allow a more accurate description of tissue residency genes. Cell types captured from the woodchuck liver and PBMCs largely separated into unique populations, except for basophils, plasmablasts, and mature B cells (Fig. 2B-E, Fig. S4A-F). Our analysis yielded numerous immune tissue residency markers in woodchuck liver. Just as in human datasets,[1,2] tissue-resident immune cells had distinct gene expression profiles from circulating populations of the same cell type (Fig. 2F,G, Fig. S11, Table S3). Liver-resident T cell and NK cell populations (Fig. 2F) had clear markers of tissue residency (e.g. *CXCR6, ITGAE, ITGB1, CCL5*)[19,20] and differentiation (e.g. *RUNX2, KLF2, TOX, ZBE2, NR4A2*)[19,20]. In contrast, PBMC enriched T cell and NK cell populations expressed circulation (e.g. *CCR7*, *SELL*)[21] and resting (e.g. *LEF1, SATB1*)[16]

phenotypes. Further differences in gene expression by compartment were noted in the NK and NKT cell subclusters (Fig. S11), with those found in liver predominantly sharing markers of lymphocyte terminal differentiation (e.g. *GZMK, NKG7*) while expressing liver-resident T and NK cell genes (e.g. *FCER1G, GZMH/B, CD160, Znf683*). Meanwhile NK and NKT cell subclusters from PBMC differentially expressed *IL7R, BANK1, SELL-1* suggesting the adoption of a residency and differentiated phenotype in the liver.

Myeloid populations also displayed compartmentalization, with dendritic cells, basophils *(GATA4)*, and activated monocytes *(IL1B)* distributed across both sites, while macrophages *(C1QC)* and Kupffer cells *(MARCO, C1QC)* were liver-enriched (Fig. 2D). Furthermore, dendritic cells in PBMCs (Fig. 2G) expressed genes related to inflammation (e.g. *FCN1, FCN2, MSR1*)[22] while those in the liver expressed genes associated with antigen-presentation to $CD8^+$ T cells and differentiation (e.g. *CD74, TAP1, CLEC9A, BATF3, IRF8, FLT3*)[23]. Taken together, this atlas provides a platform for examining the PBMC to liver immune cell differentiation, activation and infiltration trajectories and the transcriptomic signatures of woodchuck intrahepatic cell populations.

Spatially-resolved Woodchuck Liver transcriptomics Reveal Hepatocyte Metabolic Programs

Hepatocytes exhibit zonated gene expression patterns, with periportal cells specializing in high-energy processes like cholesterol biosynthesis and oxidative metabolism, while pericentral cells focus on glycolysis and xenobiotic metabolism.[3]

Unbiased spatial transcriptomics with 55um resolution (10X Genomics 3' Visium) was applied to ascribe a geographical location to the annotated intrahepatic cells in our atlas. This approach provided spatial context to periportal and pericentral hepatocytes revealing their distinct transcriptional profiles (lobule zones annotated by a pathologist, Fig 3A-E, Tables S4, S5, and S6). Pericentral hepatocytes differentially expressed human pericentral markers (*CYP2E1*, *FETUB*, *CYP1A2*) alongside *GLUD1/GLUD2* (non-zonated in humans) and *HMGCS1* (periportal in humans), indicating partially conserved but distinct zonation patterns between species.[1,17] Using pathway analyses, we found that enriched pathways in the pericentral zones include those of xenobiotic metabolism, blood coagulation, bile transport, and demethylase activity (Fig. 3F), which is consistent with what has been recorded in the literature.[3,24]

Periportal hepatocytes in the woodchuck shared both human periportal markers *HAMP, APOC2,* and mouse orthologs *Saa1/Saa2* (Fig 3D,E*,* Table S4, S5). Pathway enrichment analysis of periportal zones from the spatial transcriptomics data revealed triglyceride regulation, alcohol binding, hormone binding, and electron respiratory chain pathway activity (Fig. 3F). Combining this evidence demonstrates strong correlations with human and mouse biology in liver zonation.

As described previously,[1,17,24] hepatocyte markers were a source of ambient RNA contamination in scRNA-seq data, indicating that they may have been damaged or otherwise influenced by the experimental protocol, limiting the ability to resolve hepatocyte transcriptional profiles in the scRNA-seq data (Fig. S12).

As expected,[1,17,24] in the Visium spatial data from 55um-diameter spots, hepatocyte signatures were dominant over those of other smaller cell types making the

localization of non-hepatocytes difficult to resolve. For example, *VWF* and *ACKR1,* markers for periportal and pericentral endothelial cells respectively (Fig. S6) have correlation coefficients of -0.01 and 0.01 with their respective zones when analysing the spatial transcriptomics data (Table S6). Other marker genes have similarly weak coefficients suggesting that co-occurring signals were not sufficiently strong enough to make any conclusions (Table S6), suggesting a higher resolution spatial approach or a probe-based approach targeting non-hepatocyte genes would be required to overcome this issue.

Examination of Woodchuck Intrahepatic Cell Function using Precision-Cut Liver Slices

To validate our annotations and characterize woodchuck cell-specific response, we stimulated woodchuck precision-cut liver slices (PCLS) *in vitro* with phorbol myristate acetate (PMA) and ionomycin before snRNA-seq analysis **(**Fig. 1C, Fig. 4A). PMA triggers receptor ligation-independent NF-kB pathway activation while ionomycin increases intracellular calcium, a critical mediator of immune activation.[25] We identified cell types based on their gene expression profiles (Fig. 4B, Table S7), and compared PMA-stimulated cell populations to their unstimulated counterparts on a per-lineage basis (Fig. 4C-G, Table S8). Generally, type I inflammation gene signatures were strongly expressed in stimulated T and myeloid cells, with mild inflammation signatures occurring in other cell types (Fig. 4D-G, Table S8). Firstly, PMA-stimulated T cells expressed known activation markers (*NFKB1, CCL3, CCL4, CCL5, TNF,* and *IL2RA)* and showed TGFβ signalling and IFNγ activation respectively (Fig. 4D-E,G, Table S8).

This response mirrored previously reported human PBMC T-cell responses to PMA/ionomycin, which showed corresponding upregulation of *IL2, IFNG, TNF-α*, and *CCL5* (RANTES).[25] Collectively, this suggests a bias towards TH1 over TH2 or TH17 responses. Stimulated myeloid populations similarly upregulated *NFKB1, TNF, IFNG, IL2RA, CCL4,* and *CCL3*, along with *IL7* (Fig. 4F,G), with pathways enriched for interferon response, inflammation, and chemokine migration (Fig. S13). Myeloid-specific activation markers *SLAMF1*, *CD274*, *GBP2*, *CXCL8* and *BATF2* were also induced (Fig. S14), validating the presence of anticipated inflammatory signatures.

Beyond immune cells, hepatocytes, cholangiocytes, endothelial cells, and mesenchymal cells similarly displayed pro-inflammatory *NFKB1* pathway activation seen through upregulation of key cytokines: (*CXCL10*, *CCL4* and *CXCL8)*, and inflammatory effector proteins (*TIFA* and *IDO1)* (Fig. 4D,G, Fig. S14, Table S8). Further, stimulated hepatocytes expressed *FAS* while cholangiocytes upregulated caspase transcripts (*CASP4*, *CASP6)* (Table S8), suggesting an activation of cell-death programs in parenchymal cells. Endothelial cells also increased the expression of cell adhesion and leukocyte trafficking markers (e.g. *CD44*, *ITGAM*, *SYN3*, and *VCAM1*), Type I inflammation genes *(STAT3, IFNG)* and pro-survival genes (e.g. *BATF3*, *IRGM*, *TCF3*), underscoring the role of these cells in activating the immune response and promoting immune infiltration (Fig. 4D,G, Table S8). Furthermore, cholangiocytes and endothelial cells showed increased expression of *CSF1* (Table S8), a monocyte to macrophage differentiation growth factor. Antibody-secreting B cells, myeloid cells and hepatocytes also showed increased expression of lymphocyte growth factor gene *IL7* (Fig. 4D,G, Table S8). Altogether this suggests the upregulation of a macrophage-

promoting environment and the development of a T cell supportive niche in inflammatory liver tissue. Collectively, these findings demonstrate that woodchuck hepatic cells exhibit coordinated inflammation-associated gene activation following PMA/ionomycin stimulation.

Periportal zone damage and Cytotoxic T Cell Exhaustion in cWHV infection

To expand on the value of the woodchuck as a pre-clinical model of chronic viral liver infection, we applied our above scRNA-seq workflow to cWHV-infected woodchuck livers (Fig. 1D, Fig. 5A,B, Fig. S15-21). Using the marker genes identified through the above analysis, 23 populations of parenchymal, stromal and immune cells were annotated (Fig. S15A-F, Fig. S20-25; diseased animal characteristics Table S1; cell-type specific DGE analysis Table S9; diseased vs healthy DGE analysis for each cell type Table S10; histology Fig. S16-19). Cells from infected livers strongly and consistently expressed WHV viral transcripts while healthy samples did not (Fig. 5C-E).

Analysis of the infected spatial transcriptomics liver slices from woodchuck L215 revealed strong pericentral zonation, but very little periportal zonation suggesting a reduction of periportal gene expression in response to infection (Fig. 5F,G). Specific cell type signatures were differentially present between healthy and diseased spatial transcriptomics data (Fig. 5H) and were enriched in specific zones (Fig. 5I, Fig. S22).

We identified a cluster of T cells (CD8_Ex_TOX) with upregulation of key effector- (*IFNG, KLRD1, CCL3*), activation- (*FUT8*), and exhaustion-associated markers (*TOX, NR4A2*) in cWHV that were enriched in disease (Fig. 6A-E, Fig. S17). Additionally, NK/T cells in healthy woodchuck liver and PBMC samples had a higher

cytotoxic score while maintaining a lower exhaustion signature than cWHV NK/T cells (Fig. 6D, Table S11 for gene sets). These data indicate that $CD8^+$ T cells may be exhausted in cWHV livers leading to impaired viral clearance in chronically infected samples, similarly to recent scRNA-seq mapping of cHBV infected human livers.[16]

In addition, dendritic cells also expressed distinct genes in infected versus healthy cells, largely involved in differentiation or antigen presentation (e.g. *CADM1, WDFY4, IRF8, LRBA*) (Fig. 6F). Myeloid cell populations were also generally more present in the diseased spatial transcriptomics data compared to healthy with signatures scoring more strongly for classical monocytes, Kupffer cells, activated monocytes, and dendritic cells among others (Fig. 6G).

Furthermore, similar to cHBV infection[27], histological evaluation of cWHV-infected tissue identified immune infiltration, and mild hepatocytic necrosis at the periportal region while the central veins remain undamaged (Fig. S23-26). This supports the reduced periportal zonation seen in the spatial transcriptomics data (Fig. 5F). Altogether these results suggest a reduction in healthy periportal hepatocytes and increased exhausted T cells and immune filtration in the liver during cWHV infection.

Cell-level characterization of cWHV infection as a pre-clinical model of cHBV infection

To directly compare cWHV infection with cHBV, we analysed a publicly available dataset of immune-active cHBV-infected scRNA-seq data of immune cells (GSE182159).[16] Shared markers of chronic activation were identified by correlating genes upregulated in both cWHV and cHBV relative to their respective healthy controls

(Fig. 7A). The strongest correlations were observed in $CD8^+$ T cells, where shared markers included exhaustion-associated genes *TOX* and *NFATC1* as well as T cell activation markers, *TNFRSF1B, NR4A2, ITGB1 and CD27*.[16] Several of these T cell activation genes have also been shown in studies of liver resident T cells in both NASH and in cHBV infection.[28,29]

We then searched for shared enriched pathways in T cells and myeloid cells in both cWHV-infected woodchuck and HBV-infected human tissues (Fig. 7B,C). This analysis showed shared PD-1 activation, lymphocyte activation and pathways associated with myeloid activation such as “IFNG signalling” in chronic WHV carriers - reinforcing the parallels between cWHV and cHBV. This analysis indicates that cWHV-infected woodchuck livers exhibit disease related pathway activation that have been noted in human cHBV infection.

Previously, PD-1, a programmed cell death receptor that is expressed on activated effector T cells, has been shown to increase intrahepatically as a result of cWHV infection when analysed with quantitative polymerase chain reaction (qPCR).[30] To expand on the PD-1 shared pathway to delineate exhaustion *vs*. activation, we further examined key activation and exhaustion genes and found that in both scenarios, cHBV and cWHV T cells upregulated genes involved in exhaustion and inflammation (*TIGIT, TOX, TNFRSF9, CTLA4, IFNG, CXCR6*) (Fig. 7D, Fig. S27A-E). These findings suggest that similar programs are activated in both cWHV and HBV infections and highlights the potential and value of the woodchuck model for testing immunomodulatory interventions to drive antiviral immunity and promoting a functional cure for HBV.

Discussion

A key challenge in applying the WHV-infected woodchuck model for understanding HBV immunopathogenesis and targeting the intrahepatic cellular ecosystem in WHV disease has been the lack of molecular biology tools leveraged to understand the cellular ecosystems within the woodchuck liver and circulating immune populations.[30–32] Here, we generated the first single-cell atlas of the woodchuck liver and PBMCs and applied this map to highlight shared cell populations and gene pathways between WHV-induced disease in woodchucks and HBV infection in humans. Our atlas strengthens and reaffirms the translational potential of this unique, HBV-homologous model and will allow for the examination of key molecular parallels between WHV and human HBV pathogenesis to inform future therapeutic development.

Our cell-level examination of the parenchymal and non-parenchymal ecosystem in the healthy and diseased woodchuck liver delivers an unbiased snapshot of the major cell types in the woodchuck liver, which compliments previous woodchuck studies and adds a new level of information regarding cell level interactions that may be targeted to promote antiviral responses. For example, previous bulk RNA-seq analyses have identified intrahepatic expression of markers associated with T cell exhaustion and inhibition of anti-viral cytokine signalling in livers of woodchucks with cWHV hepatitis.[31,33] Here, we describe the transcriptome of a cWHV-infected liver derived exhausted-like T cell populations associated with viral persistence (expressing *TOX, TIGIT, CXCR6*) and found only in small populations in the healthy woodchuck liver or PBMCs. Importantly, our data suggests shared dynamics of T cell response in cWHV

and HBV thereby reinforcing the value of this model for future immune modulating studies to induce potent antiviral immunity facilitating sterilizing HBV clearance. Indeed, restoring the function of exhausted T cells through reprogramming their metabolism is thought to be a promising therapeutic target for cancer immunotherapy.[34]

Previous studies that employed qPCR to profile the immune infiltrates in biopsies from WHV infected woodchucks have implicated intrahepatic Tregs in regulating, and specifically inhibiting, the response to HBV.[30,33] We found that intrahepatic Tregs in the woodchuck liver are characterized by the expression of *FOXP3* and inhibitory genes *TOX* and *TIGIT*, in addition to upregulating the PD-1 pathway. Myeloid and dendritic cells have also been suggested to be involved in the immunopathogenesis of cWHV infection, noting an increase in their proportions weeks after infection.[30] However, myeloid cells in the infected liver have demonstrated toll-like receptor suppression suggesting an inhibition of the innate immune function.[35]

In our study, in addition to the T cell exhaustion and inhibitory signatures that were identified, our analysis simultaneously found pathways associated with the myeloid regulation of T cells. This further suggests that myeloid cells play an important role in guiding the T cell response to viral infection. Taken together, our data shows shared myeloid activation and T cell dysfunction in WHV and may provide a rationale for targeting T cell and myeloid interactions as potential a pathway to modify to limit WHV-induced T cell exhaustion and viral persistence.

We applied spatial transcriptomics profiling to probe hepatocyte zonation within the woodchuck liver, identifying pericentral (*CYP2E1, FETUB, HMGCS1*) and periportal (*APOC2, Saa1/Saa2, HAMP*) markers, which scRNA-seq alone was unable to

distinguish. As an indication of the applicability of the WHV model to examine immune targets in HBV, our study found that most immune cells in woodchuck liver and PBMCs resembled human counterparts, including T cell, monocyte and macrophage subsets, supporting translatable immune targets. Notably, tumour-associated exhausted T cells represent a promising therapeutic target given their important role in promoting viral tolerance and immune escape in many cancers.[13]

A well-described challenge related to transcriptionally profiling total liver homogenates is the fragility of hepatocytes which leads to high cell death and consequent release of ambient RNA, which can contaminate cell preparations and complicate annotation. Filtering the liver homogenate datasets with DropletQC greatly improved the clarity of signals from the liver tissue data and removed clusters previously thought to be periportal hepatocytes and Kupffer cells.

However, the WHV-infected woodchuck model of HBV is not without its caveats. cHBV infection in humans is frequently associated with progressive liver fibrosis or cirrhosis which is infrequent in woodchuck with cWHV.[12] Moreover, progression to cWHV-induced HCC is more consistent and rapid,[12] whereas only 10-25% of chronically HBV infected individuals develop HCC[36]. Finally, WHV frequently integrates around the *N-myc2* locus[37], whereas HBV insertional mutagenesis is largely thought to be random.[38] Thus, findings related to WHV-triggered HCC development in woodchucks may not fully replicate processes expected to occur in HBV-induced liver cancer.

Taken together, our work characterising the immune cells in cWHV allows for hypothesis generation of potential immunotherapies that can be tested and analysed in the cWHV infection model for HBV-induced HCC. Future work may incorporate

additional disease stages, multi-omic data, and validation of predicted cellular phenotypes. Taken together, these maps will enhance the utility of the woodchuck-WHV model and benefit the HBV community by acting as a reference for examining the liver cellular microenvironment and intrahepatic immune responsiveness to test antiviral and immunotherapies through the course of WHV-induced inflammatory liver disease and HCC development.

Abbreviations

scRNA-seq = single-cell RNA sequencing

snRNA-seq = single-nucleus RNA sequencing

HCC = hepatocellular carcinoma

ATAC-seq = assay for transposase-accessible chromatin using sequencing

PBMC = peripheral blood mononuclear cell

HBV = hepatitis B virus

WHV = woodchuck hepatitis virus

HSC = hepatic stellate cell

LSEC = liver sinusoidal endothelial cell

PCLS = precision cut liver slice

DE = differentially expressed

GSEA = Gene Set Enrichment Analysis

TLH= Total Liver Homogenate

Figure Legends

Fig. 1: Generation of the healthy woodchuck liver atlas and its application to cWHV/cHBV. (A) Intrahepatic cells (8 healthy livers) and PBMCs (7 matched samples) underwent scRNA-seq, quality filtering, and clustering/annotation. (B) Spatial transcriptomics data from 1 healthy liver (2 slices) were processed with 10X Genomics pipeline and zonation signatures characterized. (C) PCLS data were stimulated with PMA/Ionomycin followed by single-nucleus RNA sequencing, downsampling and compared to unstimulated data. (D) scRNA-seq (8 liver samples, 8 PBMCs) and spatial transcriptomics (1 liver, 2 slices) were performed on cWHV cells. The scRNA-seq samples were merged with healthy cells and compared to HBV-infected liver data[16].

Fig. 2: Woodchuck liver and PBMCs show distinct populations of circulating and tissue-resident immune cells. (A) A total UMAP of 77,338 cells from woodchuck liver biopsies (n=6), liver homogenate from perfused caudate lobes (n=2), and PBMC (n=7) with annotations assigned and coarse cell types used for subclustering circled. (B) Total UMAP colored by tissue type. (C-E) Zoom-in subclustering of NK cells and T cells (C), Myeloid cells (D) and B cells (E) (clusters from total map included in each zoom-in are indicated in Fig. 2A), upper panels show UMAPs colored by tissue type, lower panels show annotated clusters for each zoom in. (F-G) Volcano plots showing the expression of tissue residency (right) and PBMC-associated (left) genes in subclustered immune cells from woodchuck liver and PBMC, with key human genes highlighted. The 4 individual T cell and NK cell volcano plots include clusters from 2C with keywords CD4,

CD8, gd and NK in annotation, respectively; The 2 myeloid volcano plots include clusters from 2D with keywords DC and Mono in annotation respectively.

Fig. 3: Spatial transcriptomics data describes zonation patterns in the woodchuck liver. Spatial transcriptomics of 2 healthy woodchuck liver slices. (A) H&E-stained liver with pericentral/periportal zonation. (B) Spatial clusters projected onto the liver slice. (C) Key pericentral genes (*CYP2E1, FETUB, HMGCS1*) and gene score and (D) periportal genes (*APOC2, Saa1/Saa2, HAMP*) and gene score mapped onto slices. (E) Spatial clusters and key spatial-associated genes projected as dotplots. (F) Pathways upregulated for periportal (red) and pericentral (blue) hepatocytes. **AMY2B* truncated from *AMY1A;AMY1C;AMY1B;AMY2A;AMY2B*.

Fig. 4. PMA/Ionomycin stimulates immune cell populations in the woodchuck liver. (A) Healthy woodchuck precision cut liver slices were stimulated with PMA/ionomycin and single-nucleus RNA sequencing was performed. (B) A UMAP of 9,208 stimulated and unstimulated woodchuck liver cells split by treatment and labelled by cell type. (C) A barplot of sample IDs as distributed across clusters labelled in (B) where UMAPs are split by treatment (PMA/ionomycin and control, respectively). (D) UMAPs of stimulated woodchuck liver cells split by sample ID with heatmaps of key inflammatory genes projected onto the maps. (E) and (F) are volcano plots of the results of a differential expression test comparing slices stimulated by PMA/Ionomycin to unstimulated cells. (E) is a volcano plot of CD3+ NK/T cells, and (F) is a volcano plot of CD68+ myeloid cells. (G) Heatmaps showing the expression of housekeeping genes

and genes stimulated by PMA/Ionomycin. **CCL3* truncated from *CCL3L1;CCL3L3;CCL3;CCL18* and *CCL4* truncated from *CCL4L2;CCL4L1;CCL4*.

Fig. 5: A comparison of cWHV and healthy parenchymal and stromal cells. (A) UMAP of healthy and cWHV liver and PBMC cells. (B) Cells split by disease state. (C) Normalized WHV expression across woodchucks. (D) The expression of WHV in spatial transcriptomics data. (E) DE genes in infected (right) vs healthy (left) hepatocytes. (F) The distribution of periportal and pericentral scores in healthy and infected spatial transcriptomics data and (G) across liver lobule spots. (H) Cell type scores in diseased and healthy spatial data and (I) the distribution of the zonation score within spots representing each cell type (Wilcoxon test).

Fig. 6: The immune landscape of WHV-infected woodchuck blood and liver compartments. (A) A UMAP of healthy and diseased NK/T cells. (B) T cells from (A) split by disease state. (C) Proportion of immune cells within $CD45^+$ population. (D) A comparison of exhaustion and cytotoxicity scores. (E) A comparison of log-fold change and the proportion of cells that express a particular gene between $CD8^+$ Teff Mem (left) and Tox^+ Tex (right) and (F) infected (right) vs (left) healthy DCs. (G) Cell type signatures across healthy and diseased cell subtypes in visium data.

Fig. 7: Shared pathways of T cell exhaustion and activation in cWHV- and cHBV-infected tissue. (A) The average log2FC of each gene in the infected HBV and cWHV samples relative to their respective controls (red indicates significant in woodchuck, blue

indicates significant in cHBV immune-active, purple indicates significant in both) across cell types. (B) Overlapping enriched pathways in gene-set enrichment analysis between T cells from cHBV (n=5)[16] and cWHV (n=8) livers. (C) Overlapping enriched pathways in gene-set enrichment analysis between infected myeloid populations. (D) UMAPs depicting the average normalized expression of exhaustion genes in both human and woodchuck.

Acknowledgements:

The authors acknowledge the Princess Margaret Genomics Centre, the Pathology Research Program and the Advanced Optical Microscopy Facility at University Health Network for their support and services. The graphical abstract and select figures were created with Biorender.com.

References

[1] MacParland SA, Liu JC, Ma X-Z, et al. Single cell RNA sequencing of human liver reveals distinct intrahepatic macrophage populations. Nat Commun 2018;9:4383. https://doi.org/10.1038/s41467-018-06318-7.

[2] Aizarani N, Saviano A, Sagar, et al. A human liver cell atlas reveals heterogeneity and epithelial progenitors. Nature 2019;572:199–204. https://doi.org/10.1038/s41586-019-1373-2.

[3] Halpern KB, Shenhav R, Matcovitch-Natan O, et al. Single-cell spatial reconstruction reveals global division of labour in the mammalian liver. Nature

2017;542:352–6. https://doi.org/10.1038/nature21065.

[4] Michalopoulos GK. Liver regeneration after partial hepatectomy: critical analysis of mechanistic dilemmas. Am J Pathol 2010;176:2–13. https://doi.org/10.2353/ajpath.2010.090675.

[5] Global HIV, Hepatitis and STIs Programmes (HHS), Health Product Policy and Standards (HPS) WHO. Global hepatitis report 2024: action for access in low- and middle-income countries. World Health Organization; 2024.

[6] Guo W-N, Zhu B, Ai L, Yang D-L, Wang B-J. Animal models for the study of hepatitis B virus infection. Zool Res 2018;39:25–31. https://doi.org/10.24272/j.issn.2095-8137.2018.013.

[7] Unable to find information for 7600413 n.d.

[8] Menne S, Cote PJ. The woodchuck as an animal model for pathogenesis and therapy of chronic hepatitis B virus infection. World J Gastroenterol 2007;13:104–24.

[9] Michalak TI. Naturally occurring immunopathogenic model of HBV Infection, hepatitis B and HBV-associated hepatocellular carcinoma in the North American woodchuck, *Marmota monax*. J Immunol 2025.

[10] Suresh M, Menne S. Recent drug development in the woodchuck model of chronic hepatitis B. Viruses 2022;14. https://doi.org/10.3390/v14081711.

[11] Mauda-Havakuk M, Mikhail AS, Starost MF, et al. Imaging, pathology, and immune correlates in the woodchuck hepatic tumor model. J Hepatocell Carcinoma 2021;8:71–83. https://doi.org/10.2147/JHC.S287800.

[12] Michalak TI. Diverse Virus and Host-Dependent Mechanisms Influence the

Systemic and Intrahepatic Immune Responses in the Woodchuck Model of Hepatitis B. Front Immunol 2020;11:853. https://doi.org/10.3389/fimmu.2020.00853.

[13] Liu LY, Ma X-Z, Ouyang B, et al. Nanoparticle uptake in a spontaneous and immunocompetent woodchuck liver cancer model. ACS Nano 2020;14:4698–715. https://doi.org/10.1021/acsnano.0c00468.

[14] Hao Y, Hao S, Andersen-Nissen E, et al. Integrated analysis of multimodal single-cell data. BioRxiv 2020. https://doi.org/10.1101/2020.10.12.335331.

[15] Muskovic W, Powell JE. DropletQC: improved identification of empty droplets and damaged cells in single-cell RNA-seq data. Genome Biol 2021;22:329. https://doi.org/10.1186/s13059-021-02547-0.

[16] Zhang C, Li J, Cheng Y, et al. Single-cell RNA sequencing reveals intrahepatic and peripheral immune characteristics related to disease phases in HBV-infected patients. Gut 2023;72:153–67. https://doi.org/10.1136/gutjnl-2021-325915.

[17] Andrews TS, Atif J, Liu JC, et al. Single-Cell, Single-Nucleus, and Spatial RNA Sequencing of the Human Liver Identifies Cholangiocyte and Mesenchymal Heterogeneity. Hepatol Commun 2022;6:821–40. https://doi.org/10.1002/hep4.1854.

[18] 10x Genomics. PBMCs from a Healthy Donor: Whole Transcriptome Analysis, Single Cell Gene Expression Dataset by Cell Ranger 4.0.0 2020. https://support.10xgenomics.com/single-cell-gene-expression/datasets/4.0.0/Parent_NGSC3_DI_PBMC (accessed May 20, 2024).

[19] Tietscher S, Wagner J, Anzeneder T, et al. A comprehensive single-cell map of T

cell exhaustion-associated immune environments in human breast cancer. Nat Commun 2023;14:98. https://doi.org/10.1038/s41467-022-35238-w.

[20] Kumar BV, Ma W, Miron M, et al. Human Tissue-Resident Memory T Cells Are Defined by Core Transcriptional and Functional Signatures in Lymphoid and Mucosal Sites. Cell Rep 2017;20:2921–34. https://doi.org/10.1016/j.celrep.2017.08.078.

[21] Weinreich MA, Takada K, Skon C, Reiner SL, Jameson SC, Hogquist KA. KLF2 transcription-factor deficiency in T cells results in unrestrained cytokine production and upregulation of bystander chemokine receptors. Immunity 2009;31:122–30. https://doi.org/10.1016/j.immuni.2009.05.011.

[22] Wang Z, Wang Y, Yan Q, et al. FPR1 signaling aberrantly regulates S100A8/A9 production by CD14+FCN1hi macrophages and aggravates pulmonary pathology in severe COVID-19. Commun Biol 2024;7:1321. https://doi.org/10.1038/s42003-024-07025-4.

[23] Helft J, Anjos-Afonso F, van der Veen AG, Chakravarty P, Bonnet D, Reis e Sousa C. Dendritic cell lineage potential in human early hematopoietic progenitors. Cell Rep 2017;20:529–37. https://doi.org/10.1016/j.celrep.2017.06.075.

[24] Andrews TS, Nakib D, Perciani CT, et al. Single-cell, single-nucleus, and spatial transcriptomics characterization of the immunological landscape in the healthy and PSC human liver. J Hepatol 2024;80:730–43. https://doi.org/10.1016/j.jhep.2023.12.023.

[25] Lee JH, Lee BH, Jeong S, et al. Single-cell RNA sequencing identifies distinct

transcriptomic signatures between PMA/ionomycin- and αCD3/αCD28-activated primary human T cells. Genomics Inform 2023;21:e18. https://doi.org/10.5808/gi.23009.

[26] Guo X, Zhang Y, Zheng L, et al. Global characterization of T cells in non-small-cell lung cancer by single-cell sequencing. Nat Med 2018;24:978–85. https://doi.org/10.1038/s41591-018-0045-3.

[27] Tang TJ, Kwekkeboom J, Laman JD, et al. The role of intrahepatic immune effector cells in inflammatory liver injury and viral control during chronic hepatitis B infection. J Viral Hepat 2003;10:159–67. https://doi.org/10.1046/j.1365-2893.2003.00412.x.

[28] Dudek M, Pfister D, Donakonda S, et al. Auto-aggressive CXCR6+ CD8 T cells cause liver immune pathology in NASH. Nature 2021;592:444–9. https://doi.org/10.1038/s41586-021-03233-8.

[29] Nkongolo S, Mahamed D, Kuipery A, et al. Longitudinal liver sampling in patients with chronic hepatitis B starting antiviral therapy reveals hepatotoxic CD8+ T cells. J Clin Invest 2023;133. https://doi.org/10.1172/JCI158903.

[30] Suresh M, Czerwinski S, Murreddu MG, et al. Innate and adaptive immunity associated with resolution of acute woodchuck hepatitis virus infection in adult woodchucks. PLoS Pathog 2019;15:e1008248. https://doi.org/10.1371/journal.ppat.1008248.

[31] Corkum CP, Wiede LL, Ruble CL-A, et al. Identification of antibodies cross-reactive with woodchuck immune cells and activation of virus-specific and global cytotoxic T cell responses by anti-PD-1 and anti-PD-L1 in experimental chronic

hepatitis B and persistent occult hepadnaviral infection. Front Microbiol 2022;13:1011070. https://doi.org/10.3389/fmicb.2022.1011070.

[32] Yan Q, Li M, Liu Q, et al. Molecular characterization of woodchuck IFI16 and AIM2 and their expression in woodchucks infected with woodchuck hepatitis virus (WHV). Sci Rep 2016;6:28776. https://doi.org/10.1038/srep28776.

[33] Fletcher SP, Chin DJ, Ji Y, et al. Transcriptomic analysis of the woodchuck model of chronic hepatitis B. Hepatology 2012;56:820–30. https://doi.org/10.1002/hep.25730.

[34] He Q-F, Xu Y, Li J, Huang Z-M, Li X-H, Wang X. CD8+ T-cell exhaustion in cancer: mechanisms and new area for cancer immunotherapy. Brief Funct Genomics 2019;18:99–106. https://doi.org/10.1093/bfgp/ely006.

[35] Williams JB, Hüppner A, Mulrooney-Cousins PM, Michalak TI. Differential Expression of Woodchuck Toll-Like Receptors 1-10 in Distinct Forms of Infection and Stages of Hepatitis in Experimental Hepatitis B Virus Infection. Front Microbiol 2018;9:3007. https://doi.org/10.3389/fmicb.2018.03007.

[36] Ozakyol A. Global epidemiology of hepatocellular carcinoma (HCC epidemiology). J Gastrointest Cancer 2017;48:238–40. https://doi.org/10.1007/s12029-017-9959-0.

[37] Chauhan R, Churchill ND, Mulrooney-Cousins PM, Michalak TI. Initial sites of hepadnavirus integration into host genome in human hepatocytes and in the woodchuck model of hepatitis B-associated hepatocellular carcinoma. Oncogenesis 2017;6:e317. https://doi.org/10.1038/oncsis.2017.22.

[38] Budzinska MA, Shackel NA, Urban S, Tu T. Cellular genomic sites of hepatitis B

virus DNA integration. Genes 2018;9. https://doi.org/10.3390/genes9070365.

Woodchuck liver and PBMCs

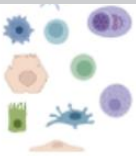

Single-cell RNA sequencing

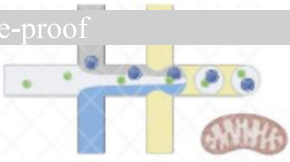

Filter cells for empty droplets and high mitochondrial levels

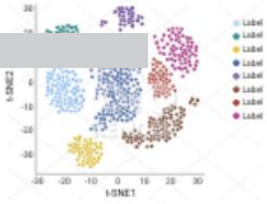

Integration, clustering, annotation
52,024 liver cells (n=8)
25,314 PBMCs (n=7)

Liver tissue frozen, cryosectioned with 16-um thickness

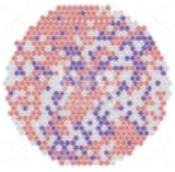

Spatial transcriptomics
5836 spots (n=2)

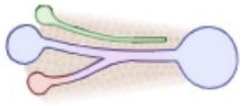

Characterize zonation signatures

Liver biopsies embedded in agarose and sliced (PCLS)

Liver slices stimulated with PMA/Ionomycin

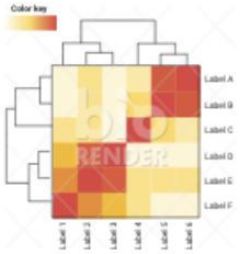

Single-nucleus RNA sequencing, downsampling and DE analysis

Woodchucks infected with woodchuck hepatitis virus (WHV)

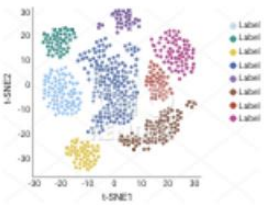

Single-cell RNA sequencing of infected liver
40,810 liver cells (n=8)
19,518 PBMCs (n=8)

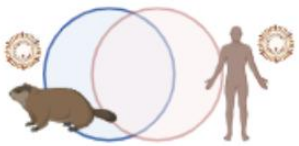

Comparison of WHV-infected woodchuck liver with HBV-infected human liver

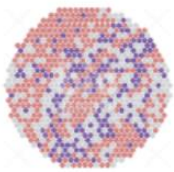

Spatial transcriptomics
4808 spots (n=2)

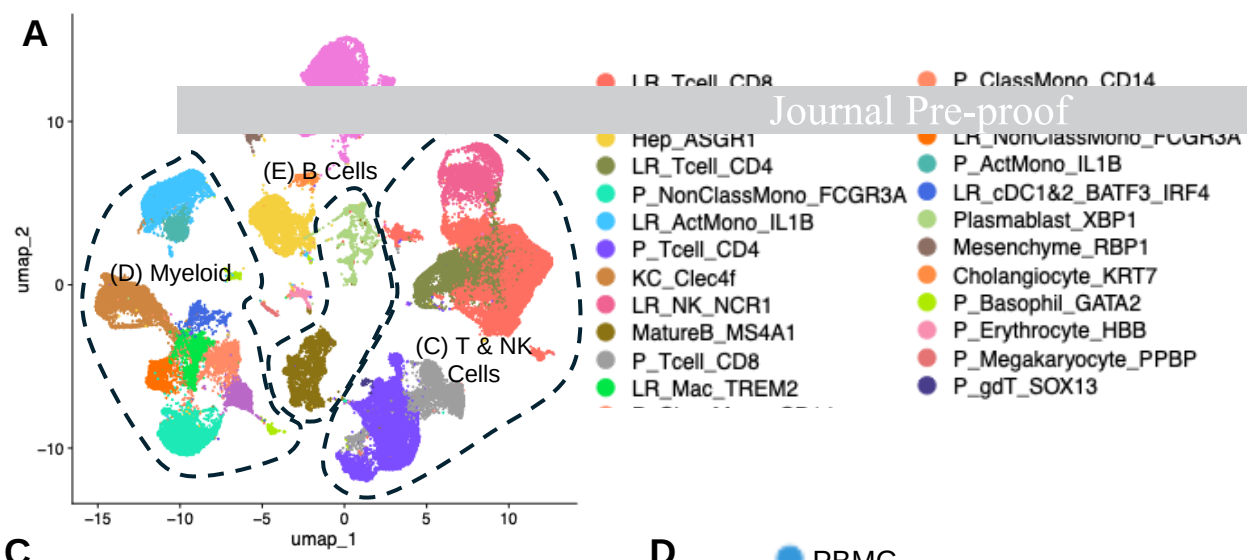

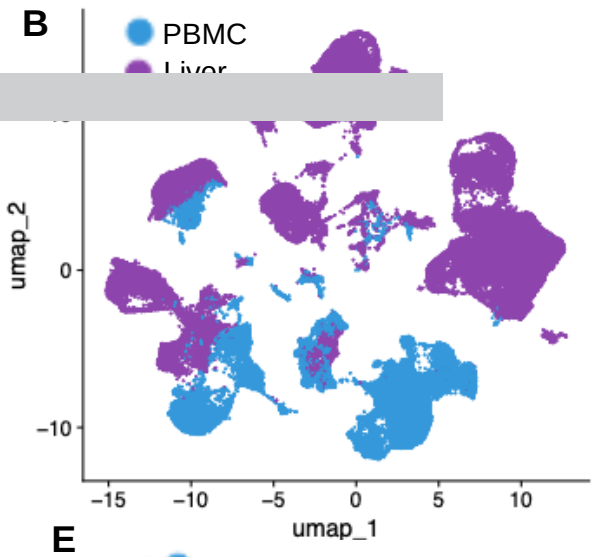

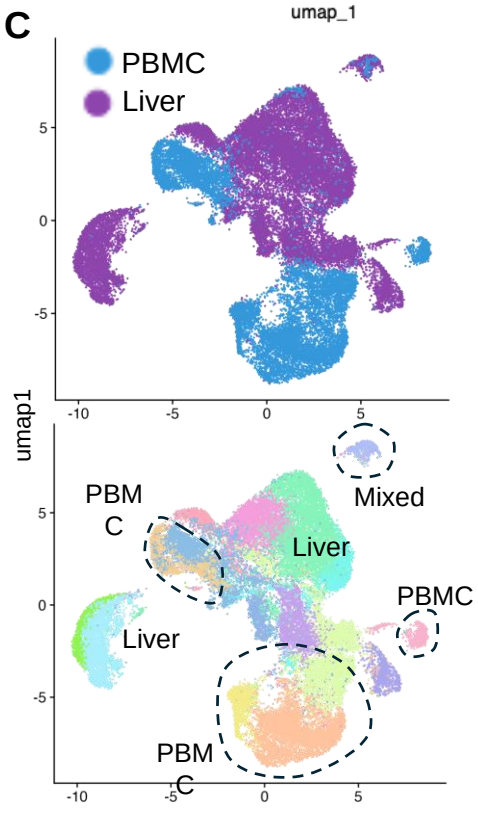

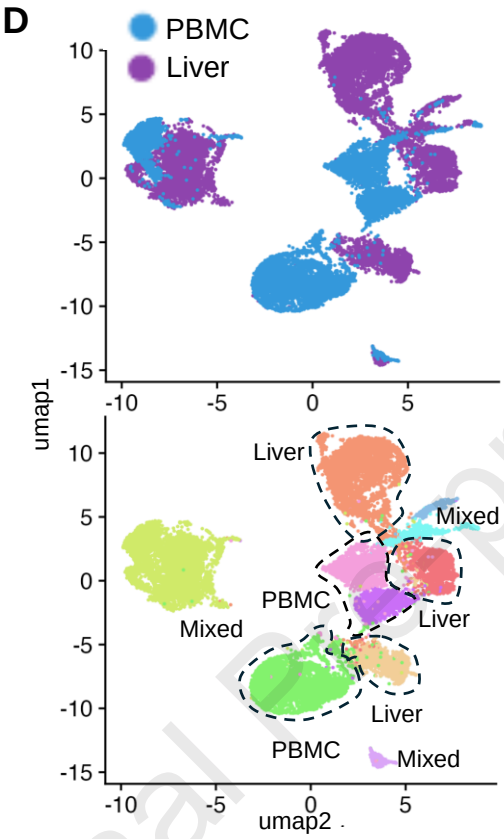

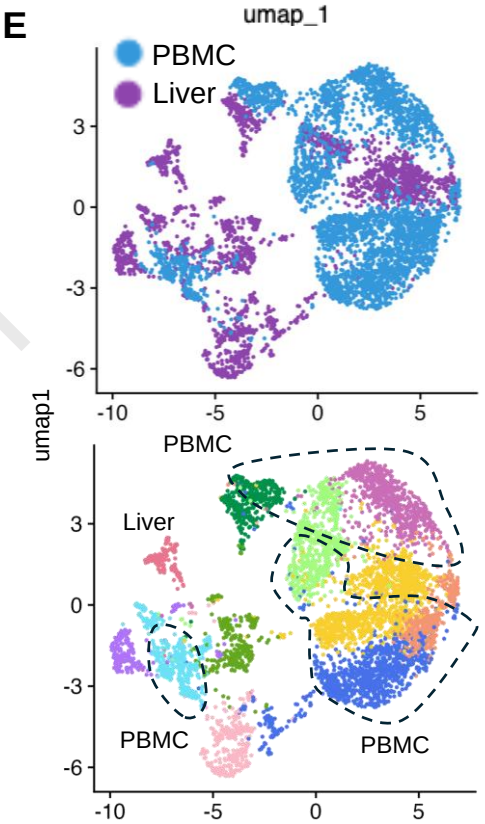

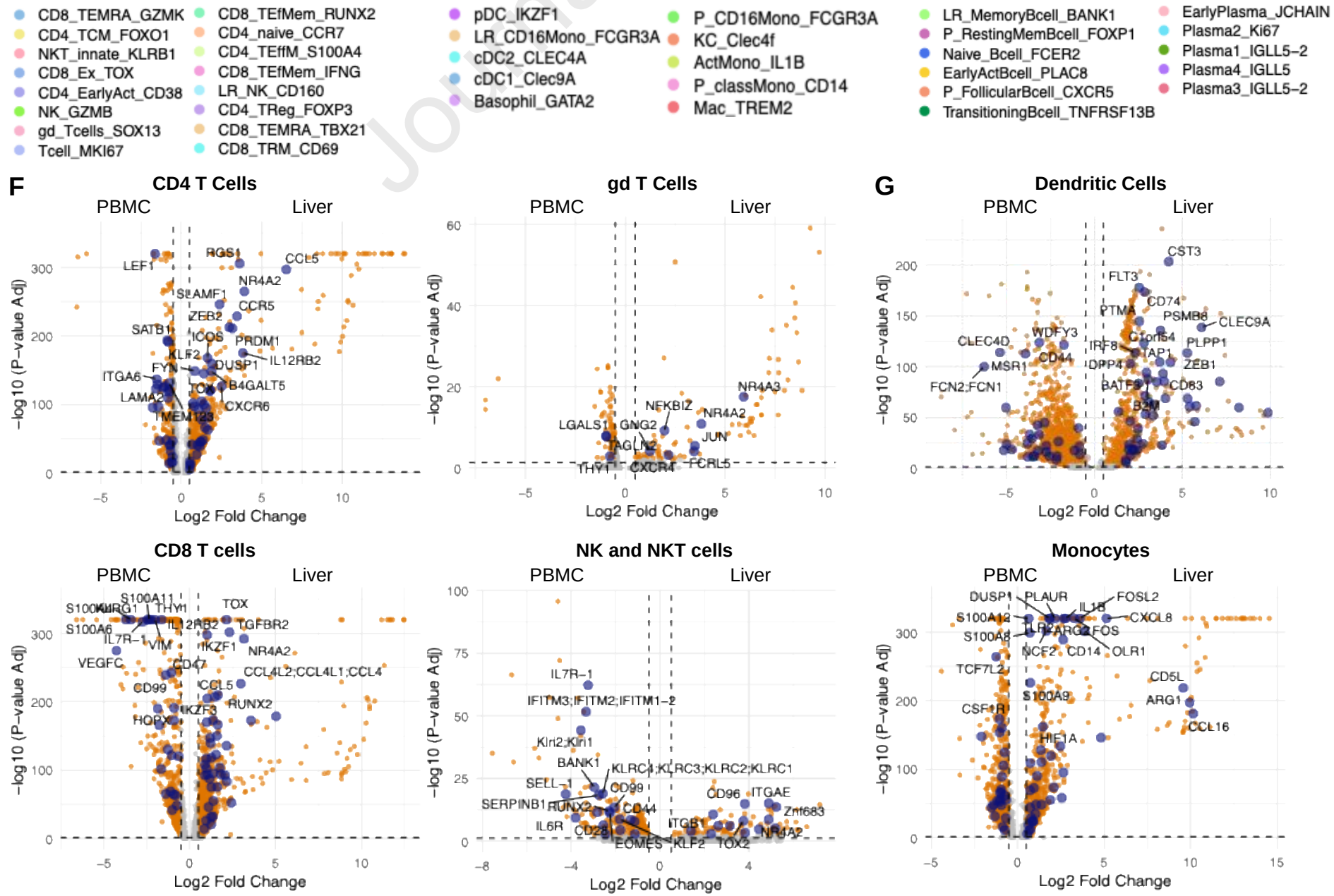

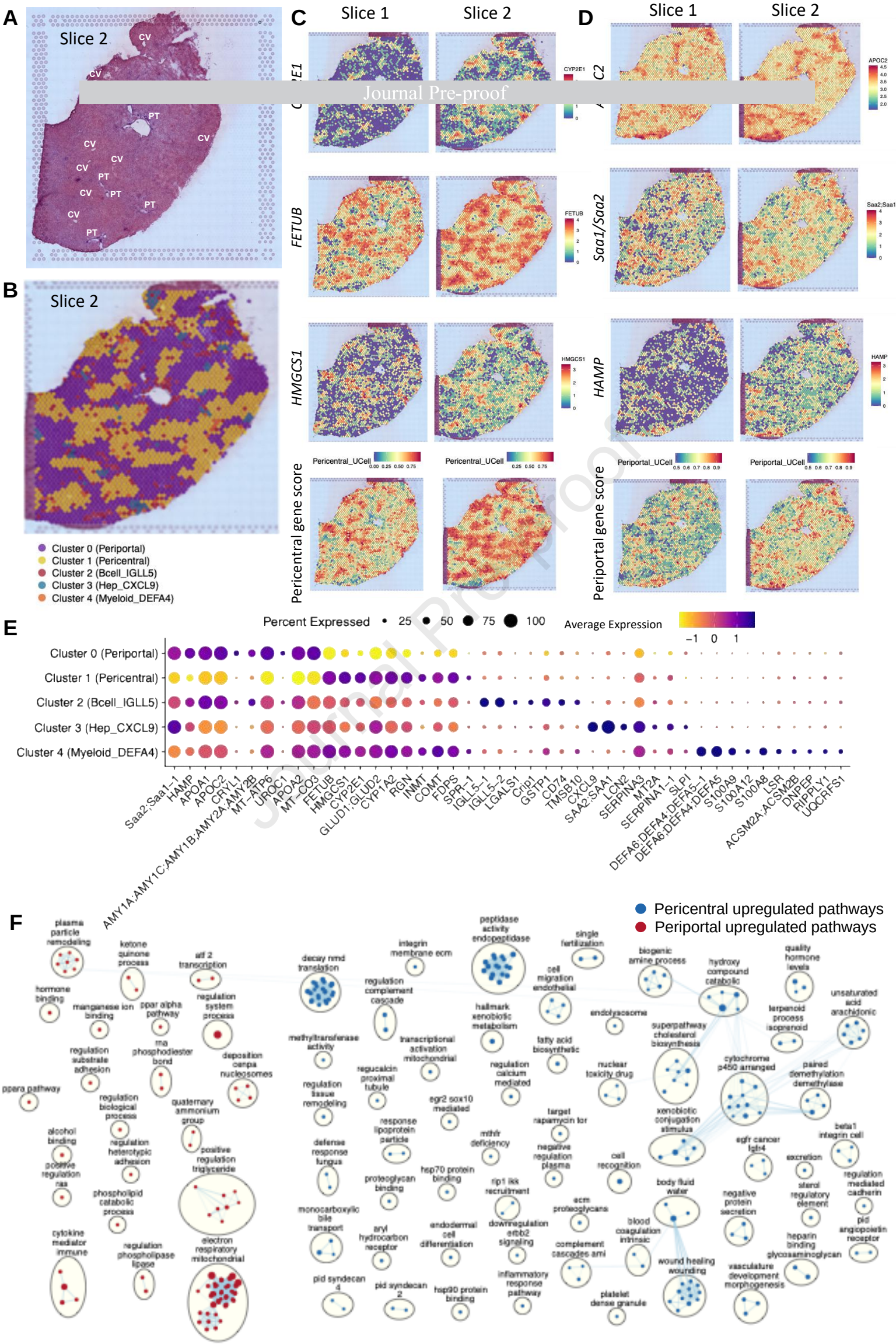

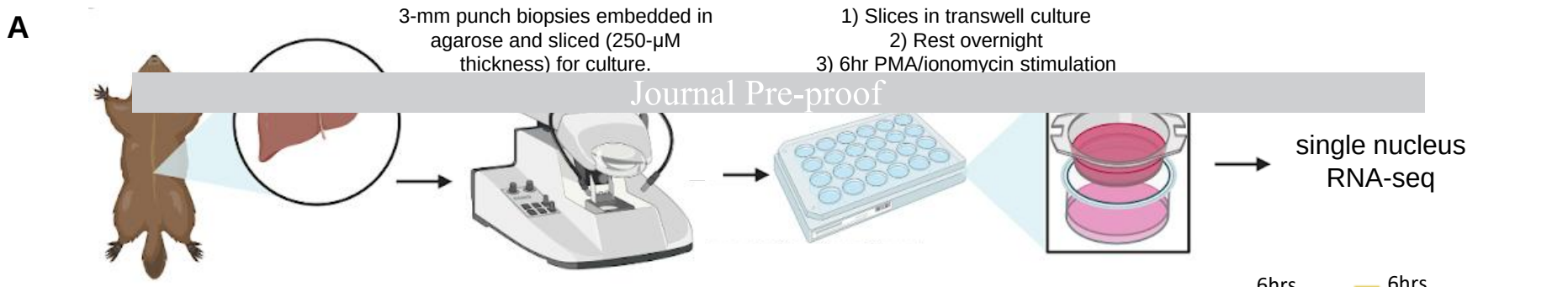

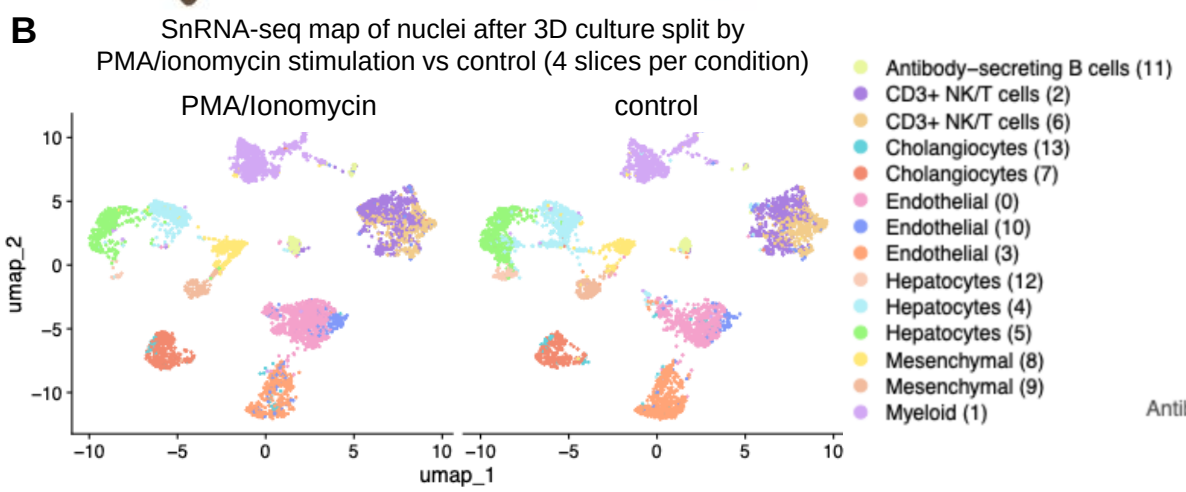

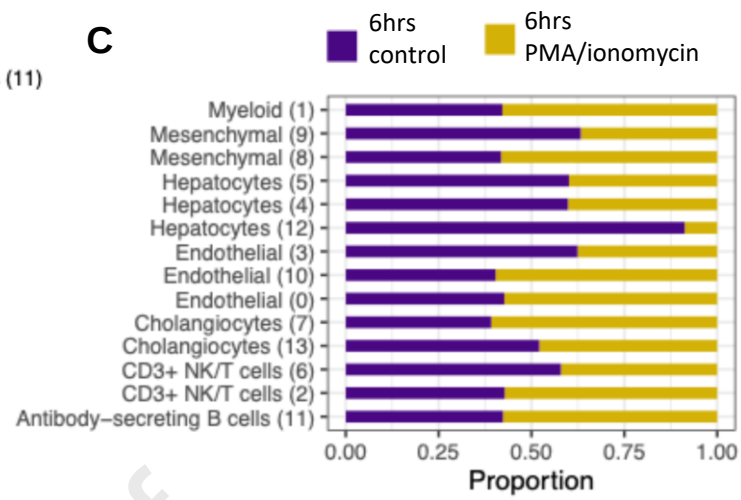

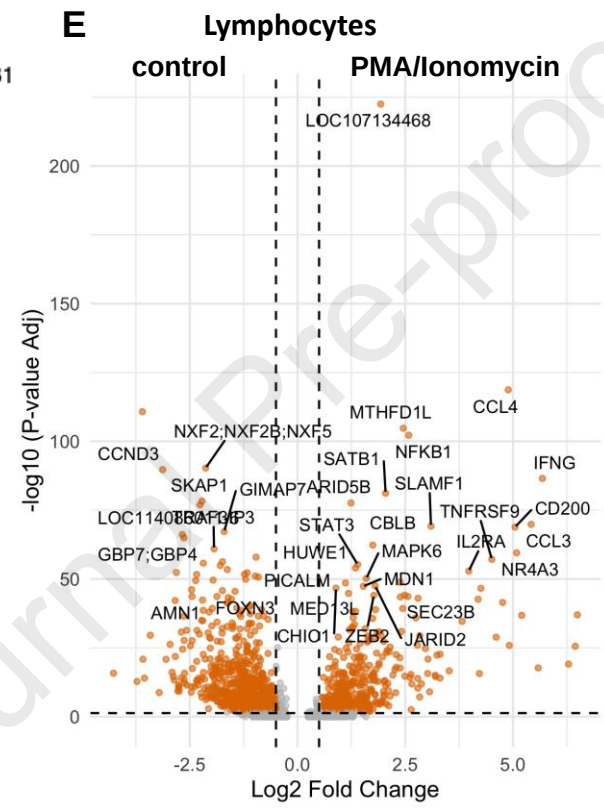

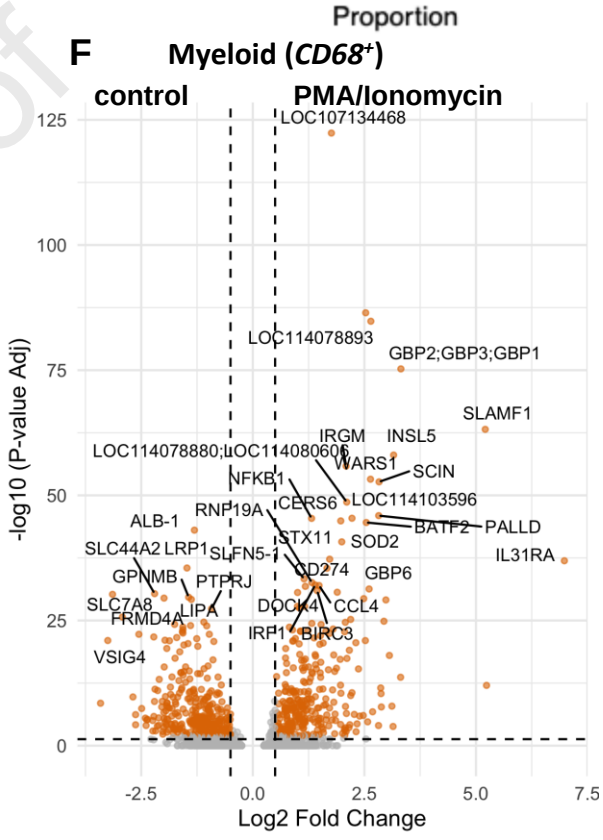

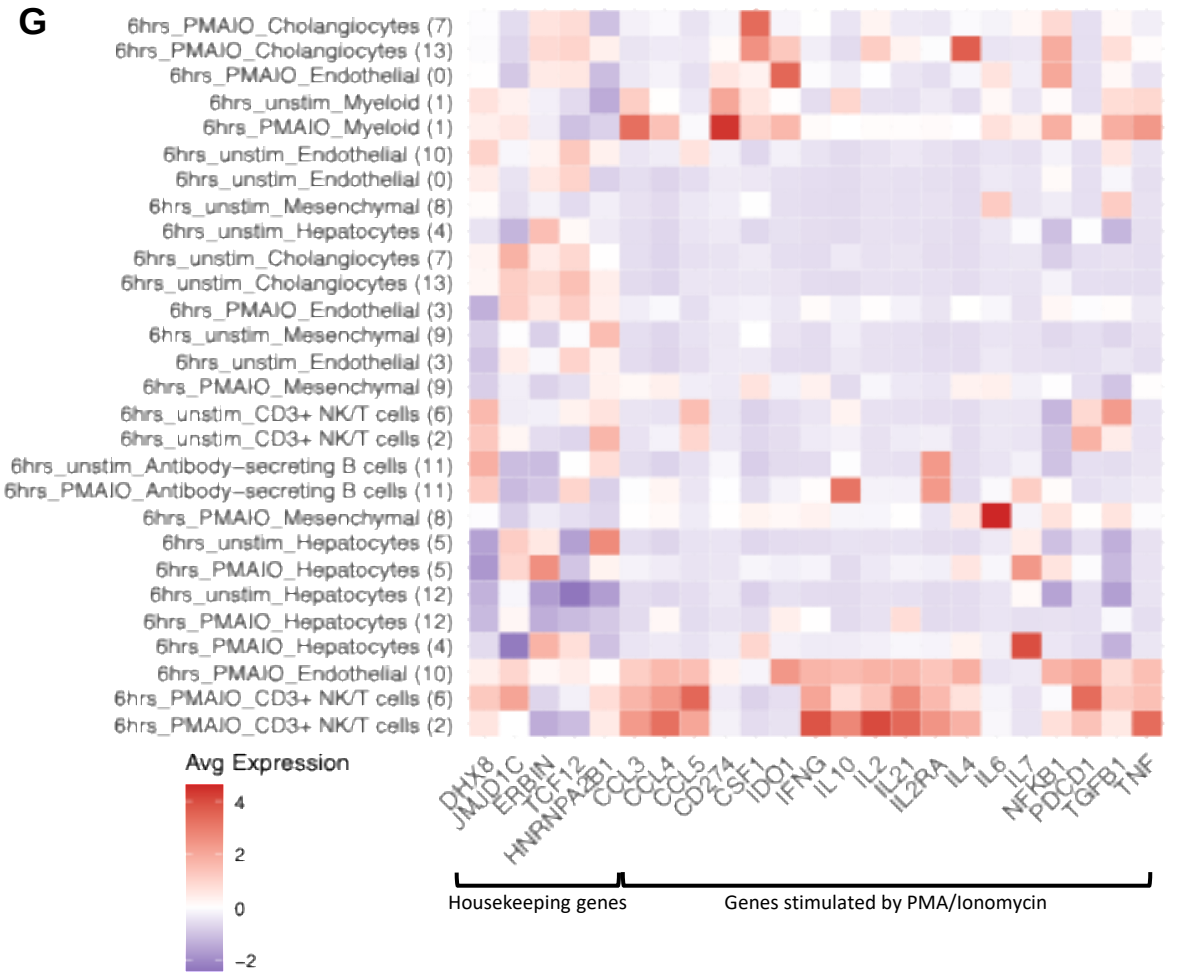

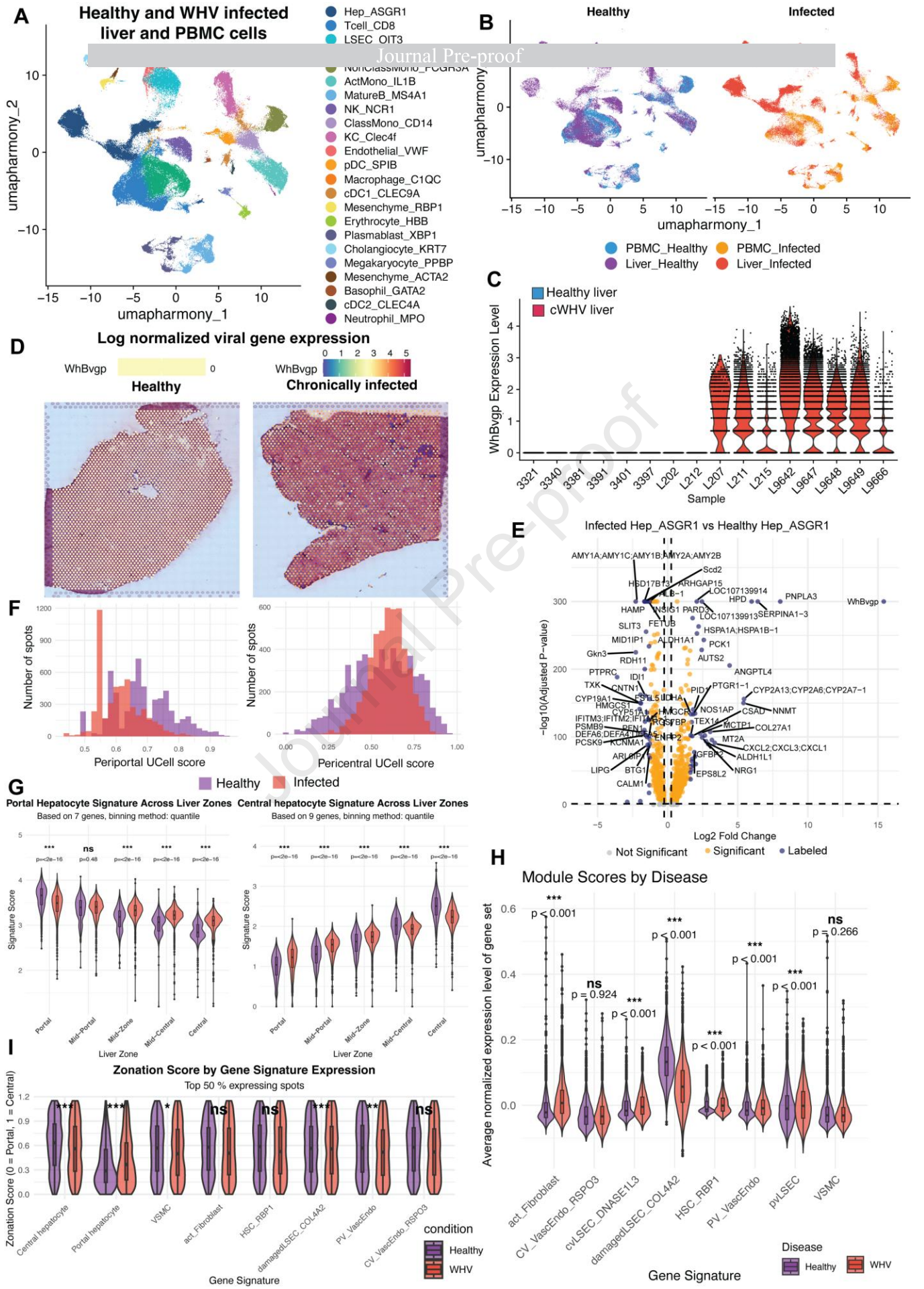

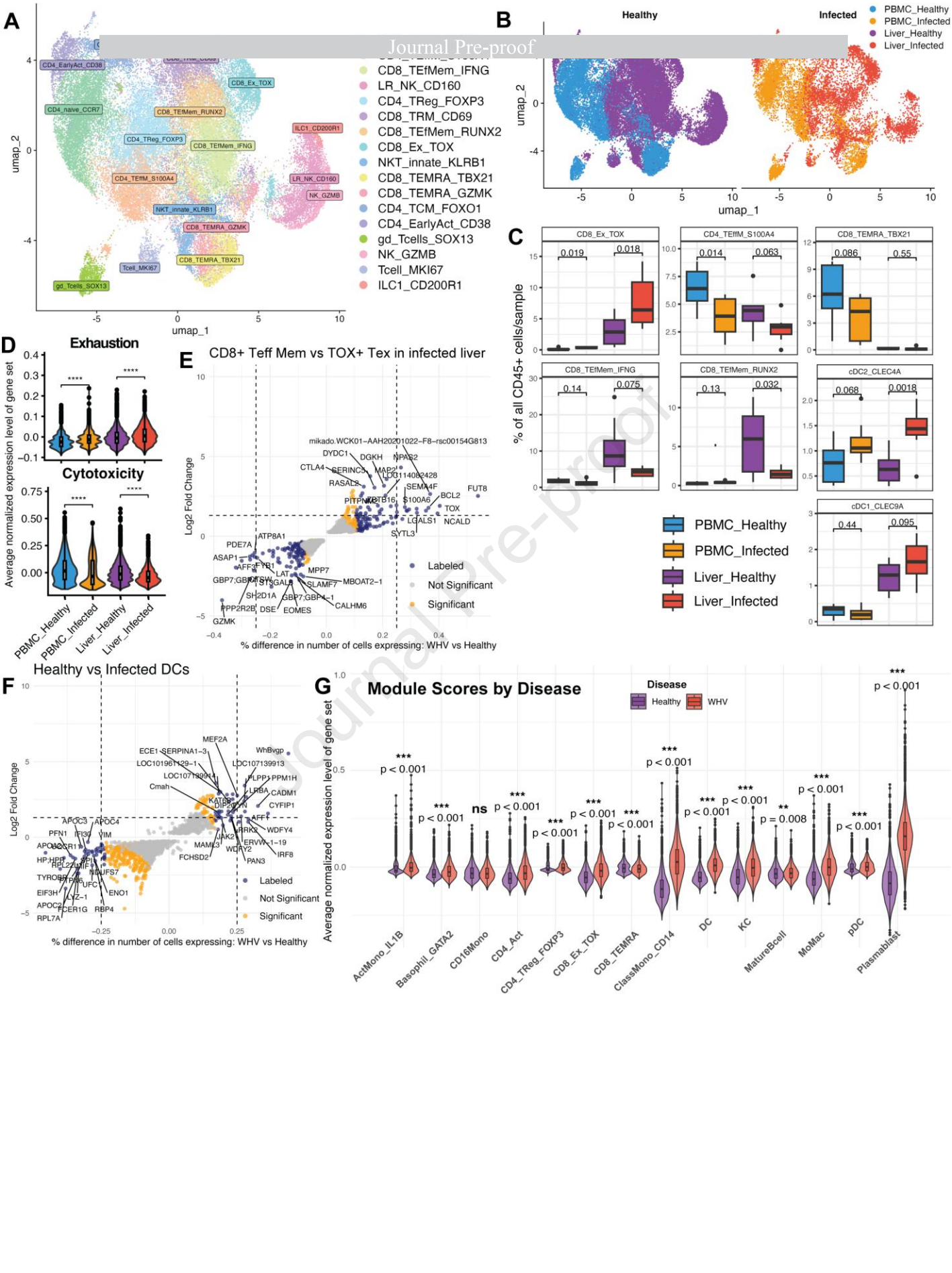

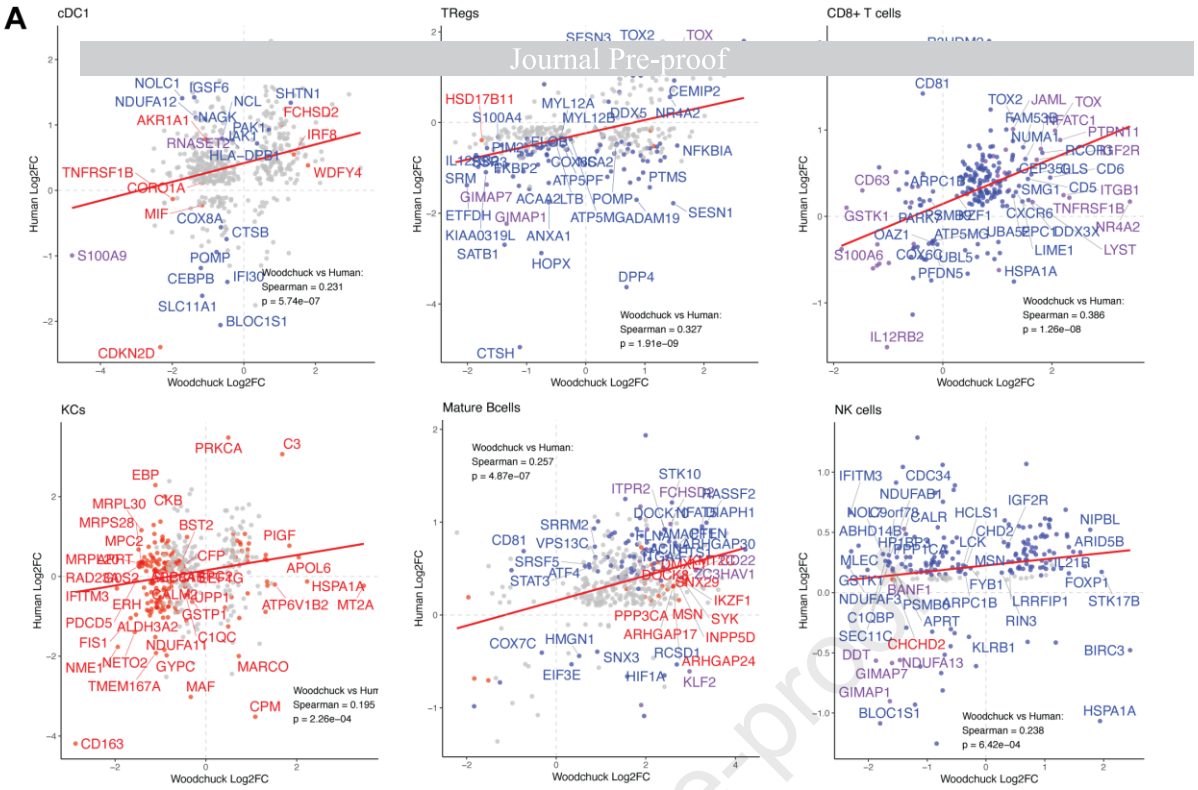

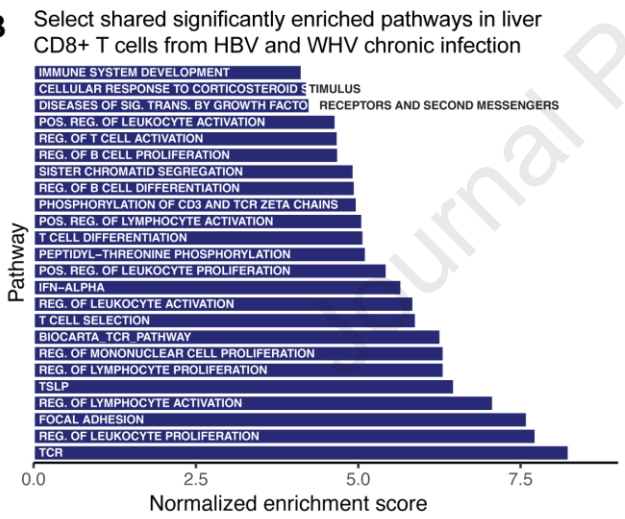

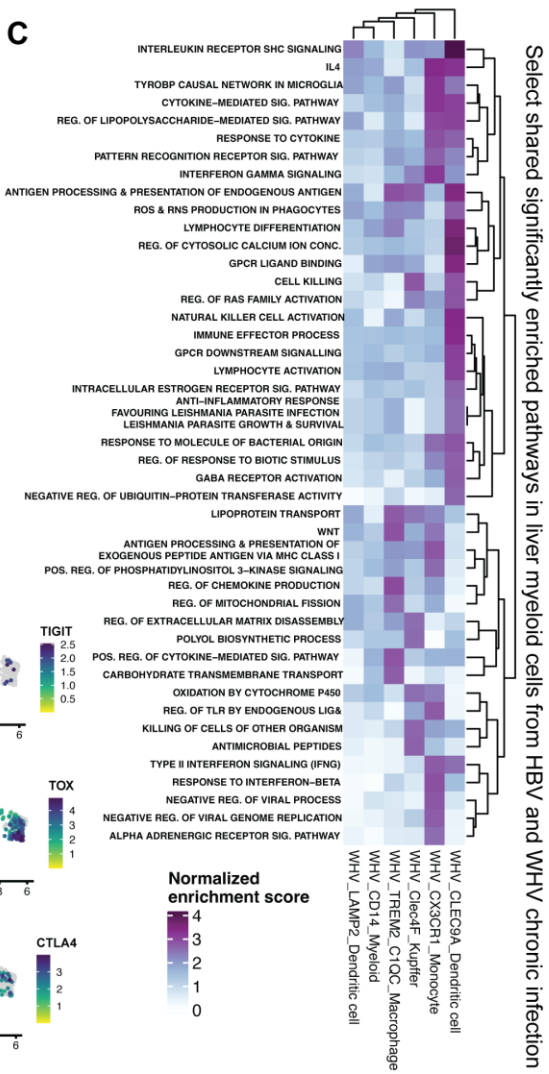

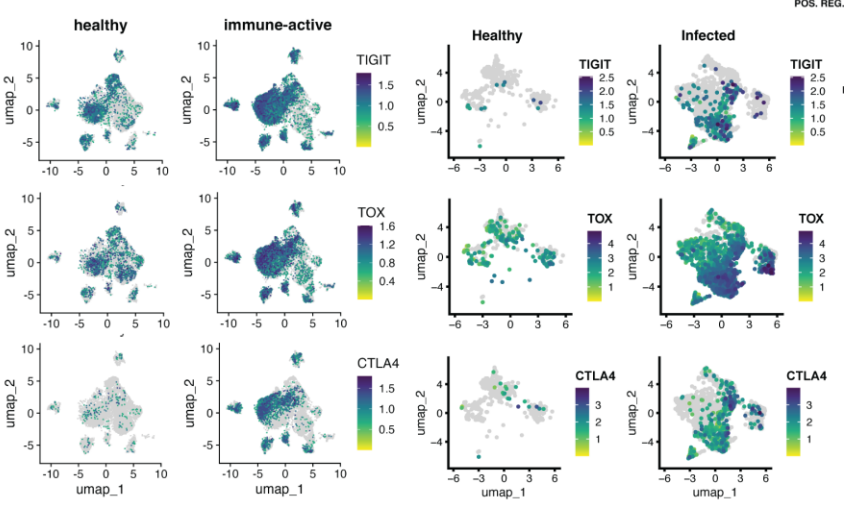

Highlights

- Woodchuck liver and blood cells share key characteristics with human cells
- Analogous cells in liver and blood have unique signatures indicating their origin
- Exhausted T cells are enriched in the diseased woodchuck liver
- Woodchuck and human share chronic hepatic inflammation gene signatures